Dynamic Mixed Mode Crack Propagation Behavior of Structural Bonded Joints

Ouk Sub Lee*, Jae Chul Park, Gyu Hyun Kim

School of Mechanical, Aerospace and Automation Engineering, InHa University

The stress field around the dynamically propagating interface crack tip under a remote mixed mode loading condition has been studied with the aid of dynamic photoelastic method. The variation of stress field around the dynamic interface crack tip is photographed by using the Cranz-Shardin type camera having 10^6 fps rate. The dynamically propagating crack velocities and the shapes of isochromatic fringe loops are characterized for varying mixed load conditions in double cantilever beam (DCB) specimens. The dynamic interface crack tip complex stress intensity factors, K_1 and K_2, determined by a hybrid-experimental method are found to increase as the load mixture ratio of y/x (vertical/horizontal) values. Furthermore, it is found that the dynamically propagating interface crack velocities are highly dependent upon the varying mixed mode loading conditions and that the velocities are significantly small compared to those under the mode I impact loading conditions obtained by Shukla (Singh & Shukla, 1996a, b) and Rosakis (Rosakis et al., 1998) in the USA.

Key Words : Dynamic Interface Crack, Propagating Velocity, Dynamic Stress Intensity Factors, Rayleigh Wave Speed, Mixed Mode Loading

1. Introduction

During the last few decades many interesting problems pertaining to dynamic crack propagation and arrest phenomena have been investigated by many researchers throughout the world (Dally, 1991; Kobayashi, 1978; Lee & Kim, 1999; Singh & Shukla, 1996a, 1996b). In recent years, there has been considerable interest in the study of dynamic bimaterial interface crack propagation from both theoretical and experimental viewpoints (Anderson, 1977; Deng, 1992; Deng, 1993). Even though the majority of these studies have been either analytical or numerical in nature, a few experimental studies on the dynamic interfacial fracture have been appeared in the

* Corresponding Author,
  E-mail : leeos@dragon.inha.ac.kr
  TEL : +82-32-860-7315 ; **FAX** : +82-32-868-1716
  School of Mechanical, Aerospace and Automation Engineering, InHa University, Inchon, 402-751, Korea.
  (Manuscript **Received** January 7, 2000; **Revised** April 11, 2000)

Technical Journals from 1991. Rosakis group at California Institute of Technology and Shukla group at University of Rhode Island are the representatives among others.

This study is motivated by the need to establish procedures and investigate the applicability of dynamic photoelasticity to study interface failure under mixed mode loading condition (Gdoutos, 1985; Mohammad, 1995), and thus, attempts to develop the framework of employing photoelasticity to observe and investigate the phenomena of dynamic interface failure. The initial failure was obtained by subjecting the bimaterial specimen to dynamic mixed mode loading. The dynamic isochromatic fringe patterns surrounding a crack tip propagating along a bimaterial interface are photographed and characterized. A parametric investigation has been carried out to study the influence of varying fracture parameters on isochromatic fringe patterns. The primary relevant fracture parameters such as the complex stress intensity factors, K1 and K2, for the stress field surrounding the dynamic interface crack tip are

extracted by using a hybrid experimental-theoretical technique.

2. Theoretical

2.1 Stress field and dynamic stress intensity factors at the dynamic interface crack tip

The stress field shown in Fig. 1 at the dynamic interface crack tip developed by Deng (Deng, 1993) are rearranged to fit the photoelastic analysis conducted in this study as below in polar coordinate system.

$$
\begin{aligned}
\sigma_{xx}(r, \theta) = &\frac{1}{\sqrt{2\pi r}}[K_1\cos(\varepsilon\ln r) \\
&- K_2\sin(\varepsilon\ln\gamma)]\overset{\wedge}{\sigma'_{xx\theta}}(\theta) \\
&+ \frac{1}{\sqrt{2\pi r}}\eta[K_1\sin(\varepsilon\ln r) \\
&+ K_2\cos(\varepsilon\ln\gamma)]\overset{\wedge}{\sigma''_{xx\theta}}(\theta) \\
&+ \frac{1}{\sqrt{2\pi r}}K_3\overset{\wedge}{\sigma'''_{xx\theta}}(\theta) \\
&+ Higher\ Order\ Terms
\end{aligned}
$$

$$
\begin{aligned}
\sigma_{yy}(r, \theta) = &\frac{1}{\sqrt{2\pi r}}[K_1\cos(\varepsilon\ln r) \\
&- K_2\sin(\varepsilon\ln\gamma)]\overset{\wedge}{\sigma'_{yy\theta}}(\theta) \\
&+ \frac{1}{\sqrt{2\pi r}}\eta[K_1\sin(\varepsilon\ln r) \\
&+ K_2\cos(\varepsilon\ln\gamma)]\overset{\wedge}{\sigma''_{yy\theta}}(\theta) \qquad (1) \\
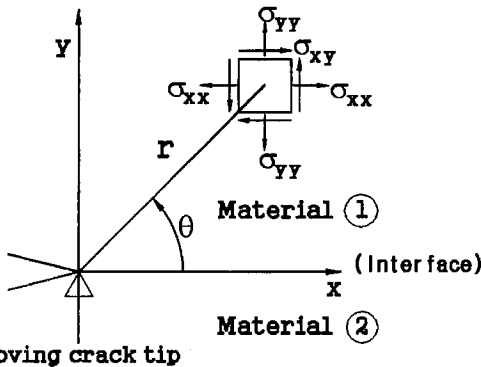&+ \frac{1}{\sqrt{2\pi r}}K_3\overset{\wedge}{\sigma'''_{yy\theta}}(\theta)
\end{aligned}
$$

Fig. 1 A coordinate system and stress component for a small element at the dynamic interface crack tip

$$
\begin{aligned}
+ &Higher\ Order\ Terms \\
\sigma_{xy}(r, \theta) = &\frac{1}{\sqrt{2\pi r}}[K_1\cos(\varepsilon\ln r) \\
&- K_2\sin(\varepsilon\ln\gamma)]\overset{\wedge}{\sigma'_{xy\theta}}(\theta) \\
&+ \frac{1}{\sqrt{2\pi r}}\eta[K_1\sin(\varepsilon\ln r) \\
&+ K_2\cos(\varepsilon\ln\gamma)]\overset{\wedge}{\sigma''_{xy\theta}}(\theta) \\
&+ \frac{1}{\sqrt{2\pi r}}K_3\overset{\wedge}{\sigma'''_{xy\theta}}(\theta) \\
&+ Higher\ Order\ Terms
\end{aligned}
$$

where r, θ=polar coordinate centered at the dynamic interfacial crack tip

ε, η, $\overset{\wedge}{\sigma_{ixe''}}(\theta)$ =functions in terms of material properties and crack propagation velocity

K_1, K_2=plane-interface-crack mixed-stress-intensity-factors

$$P = \frac{2a_la_s - (1+a_s^2)}{\mu D}, \quad Q = \frac{a_s(1-a_s^2)}{\mu D},$$

$$R = \frac{a_l(1-a_s^2)}{\mu D}$$

$$\varepsilon = \frac{P_1 - P_2}{\sqrt{(R_1+R_2)(Q_1+Q_2)}}, \quad \eta = \frac{\sqrt{P_1+P_2}}{\sqrt{Q_1+Q_2}},$$

$$\tan\theta_l = \beta_l\tan\theta, \quad \theta_l = \tan^{-1}\cdot(\beta_l\tan\theta)$$

$$\beta_l = \sqrt{(1 - \frac{v}{c_l})^2}, \quad v = \text{crack velocity}$$

$$c_l = \sqrt{\frac{(k+1)}{k-1}}\cdot\sqrt{\frac{G}{\rho}}$$

G=shear modulus, ρ=mass density

$$k = \frac{3-\nu}{1+\nu}\,(\text{plane stress}) = 3-4\nu\,(\text{plane strain})$$

ν=Poisson's ratio

$$r_l = \sqrt{\cos^2\theta + \beta_l^2\sin^2\theta}, \quad \beta_s = \sqrt{(1 - \frac{v}{c_s})^2}$$

$$c_s = \sqrt{\frac{G}{\rho}}, \quad \eta = \sqrt{\frac{R_1+R_2}{Q_1+Q_2}}$$

$$R_1 = \left[\frac{\beta_l(2-B)}{GD}\right]_1, \quad R_2 = \left[\frac{\beta_l(2-B)}{GD}\right]_2$$

$$B = 1 + \beta_s^2$$

$$Q_1 = \left[\frac{\beta_s(2-B)}{GD}\right]_1, \quad Q_2 = \left[\frac{\beta_s(2-B)}{GD}\right]_2$$

$$D_1 \equiv [4\beta_l\beta_s - (1+\beta_s^2)^2]_1,$$

$$D_2 \equiv [4\beta_l\beta_s - (1+\beta_s^2)^2]_2$$

$$\varepsilon = \frac{1}{2\pi}\ln\frac{1-\beta}{1+\beta}, \quad \beta = \frac{P_1-P_2}{\sqrt{(Q_1+Q_2)(R_1+R_2)}}$$

$$C_l(n=0, \varepsilon=\varepsilon, \eta=1) = -r_l^{-\frac{1}{2}}e^{\varepsilon(\pi-\theta_l)}[2\beta_s\cdot\eta$$

$$- (1+\beta_s^2)]\times\cos(\frac{-1}{2}\theta_l + \varepsilon\ln r_l)$$

$$S_l(n=0, \ \varepsilon=\varepsilon, \ \eta=1) = r_l^{-\frac{1}{2}} \times e^{\varepsilon(\pi-\theta_l)}[2\beta_s\eta$$
$$- (1+\beta_s^2)] \times \sin(-\frac{1}{2}\theta_l + \varepsilon\ln r_l)$$

$$C_s(n=0, \ \varepsilon=\varepsilon, \ \eta=1) = -r_s^{\frac{-1}{2}}e^{\varepsilon(\pi-\theta_s)}[2\beta_l$$
$$-\eta(1+\beta_s^2)] \times \cos(\frac{-1}{2}\theta_s + \varepsilon\ln r_s)$$

$$S_s(n=0, \ \varepsilon=\varepsilon, \ \eta=1) = r_s^{-\frac{1}{2}}e^{\varepsilon(\pi-\theta_s)}[2\beta_l$$
$$-\eta(1+\beta_s^2)] \times \sin(\frac{-1}{2}\theta_s + \varepsilon\ln r_s)$$

$$\tan\theta_s = \beta_s\tan\theta, \ r_s = \sqrt{\cos^2\theta + \beta_s^2\sin^2\theta}$$

$$\underset{\sigma'_{xx0}}{\wedge}(\theta) = \frac{1}{2D\cosh\pi\varepsilon}\{(1+2\beta_l^2-\beta_s^2)[C_l(n=0,$$
$$\varepsilon=\varepsilon, \ \eta=1) + C_l(n=0, \ \varepsilon=-\varepsilon, \ \eta=-1)]$$
$$+2\beta_s[C_s(n=0, \ \varepsilon=\varepsilon, \ \eta=1) + C_s(n=0, \ \varepsilon$$
$$=-\varepsilon, \ \eta=-1)]\}$$

$$\underset{\sigma'_{yy0}}{\wedge}(\theta) = \frac{1}{2D\cosh\pi\varepsilon}\{-(1+\beta_s^2)[C_l(n=0, \ \varepsilon=\varepsilon,$$
$$\eta=1) + C_l(n=0, \ \varepsilon=-\varepsilon, \ \eta=-1)]$$
$$+2\beta_s[C_s(n=0, \ \varepsilon=\varepsilon, \ \eta=1) + C_s(n=0,$$
$$\varepsilon=-\varepsilon, \ \eta=-1)]\}$$

$$\underset{\sigma'_{xy0}}{\wedge}(\theta) = \frac{1}{2D\cosh\pi\varepsilon}\{2\beta_l[S_l(n=0, \ \varepsilon=\varepsilon, \ \eta=1)$$
$$+ S_l(n=0, \ \varepsilon=-\varepsilon, \ \eta=-1)] + (1+\beta_s^2)$$
$$[S_s(n=0, \ \varepsilon=\varepsilon, \ \eta=1) + S_s(n=0, \ \varepsilon=-\varepsilon,$$
$$\eta=-1)]\}$$

$$\underset{\sigma''_{xx0}}{\wedge}(\theta) = \frac{1}{2D\eta\cosh\pi\varepsilon}\{(1+2\beta_l^2-\beta_s^2)[S_l(n=0,$$
$$\varepsilon=\varepsilon, \ \eta=1) - S_l(n=0, \ \varepsilon=-\varepsilon, \ \eta=-1)]$$
$$+2\beta_s[S_s(n=0, \ \varepsilon=\varepsilon, \ \eta=1) - S_s(n=0,$$
$$\varepsilon=-\varepsilon, \ \eta=-1)]\}$$

$$\underset{\sigma''_{yy0}}{\wedge}(\theta) = \frac{1}{2D\eta\cosh\pi\varepsilon}\{(1+\beta_s^2)[-S_l(n=0,$$
$$\varepsilon=\varepsilon, \ \eta=1) + S_l(n=0, \ \varepsilon=-\varepsilon, \ \eta=-1)]$$
$$+2\beta_s[-S_s(n=0, \ \varepsilon=\varepsilon, \ \eta=1) + S_s(n=0, \ \varepsilon$$
$$=-\varepsilon, \ \eta=-1)]\}$$

$$\underset{\sigma''_{xy0}}{\wedge}(\theta) = \frac{1}{2D\eta\cosh\pi\varepsilon}\{2\beta_l[-C_l(n=0, \ \varepsilon=\varepsilon,$$
$$\eta=1) + C_l(n=0, \ \varepsilon=-\varepsilon, \ \eta=-1)]$$
$$+ (1+\beta_s^2)[-C_s(n=0, \ \varepsilon=\varepsilon, \ \eta=1)$$
$$+ C_s(n=0, \ \varepsilon=-\varepsilon, \ \eta=-1)]\}$$

$$\underset{\sigma'''_{xx0}}{\wedge}(\theta) = \gamma_s^{\frac{-1}{2}}\left\{\frac{1}{a_s}\sin\frac{-1}{2}\theta_s\right\}$$

$$\underset{\sigma'''_{yy0}}{\wedge}(\theta) = \gamma_s^{\frac{-1}{2}}\left\{\cos\frac{-1}{2}\theta_s\right\}$$

Combining the stress-optics law (Dally & Riley, 1991) with $\tau_m = Nf_\sigma/2t$, we may relate the experimental results with the theoretical stress field as below.

$$(\frac{Nf_\sigma}{t})^2 = (2\tau_m)^2 = (\sigma_{xx}-\sigma_{yy})^2 + (2\sigma_{xy})^2 \quad (2)$$

where N = the experimental fringe order of the dynamic isochromatic pattern.

f_σ = the dynamic fringe constant of the photoelastic material (6.7 *kN/m-fringe* for polycarbonate)

t = the specimen thickness (=4.5 *mm*)

2.2 Characterization of isochromatic fringe loops at the dynamic interface crack tip

In this study, the Newton-Raphson method and over-deterministic least square method (OLSM) are used to extract the complex stress intensity factors, K_1, K_2 appeared in Eq. (1) for the dynamic interface crack tip stress field. To determine the stress intensity factor, K_1 and K_2, we should take experimental data at the vicinity of the crack tip to eliminate boundary effect. However, it is difficult to distinguish the experimental isochromatics data due to concentrated fringe and local plastic zone at the vicinity of the crack tip. Therefore a multi-functional determination procedure should be used to extract the more precise stress intensity factors. The functional relationship between maximum shear stress and isochromatic fringe loop may be written as.

$$F = \beta(2\tau_m)^2 - 1 = \beta[(\sigma_{xx}-\sigma_{yy})^2$$
$$+ (2\sigma_{xy})^2] - 1 = 0 \quad (3)$$

where, $\beta = (\frac{t}{Nf_\sigma})^2$

In the case we could express an equation in the functional form as

$$F_k = F(A_n, B_m) = 0 \quad (4)$$

Sanford (Sanford, 1980) developed an algorithm to determine the best A_n and B_m by using ODLS optimizing process summarized as follows:

$$(F_k)_{i+1} = (F_k)_i + (\frac{\partial F_k}{\partial A_n})_i\Delta A_n$$
$$+ (\frac{\partial F_k}{\partial B_m})_i\Delta B_m \quad (5)$$

where, i = the iteration number to obtain the best value.

A_n, B_m = the variables need to determine.

Using Eq. (5), we can get the results satisfying

$(F_k)_{i+1}=0$ in the following loop iteration equations.

$$(F_k)_{i+1}=0$$
$$(\frac{\partial F_k}{\partial A_n})_i \Delta A_n + (\frac{\partial F_k}{\partial B_m})_i \Delta B_m = -(F_k)_i$$

Changing the above to the matrix formation, we get.

$$\left[\frac{\partial F_k}{\partial A_n} \frac{\partial F_k}{\partial B_m}\right]\left[\begin{matrix}\Delta A_n \\ \Delta B_m\end{matrix}\right]=-[F_k]$$

or

$$[A][\Delta X]=[F] \qquad (6)$$

in a simple form.
where,

$$[A]=\left[\begin{matrix}\frac{\partial F_1}{\partial A_n} & \frac{\partial F_1}{\partial B_m} \\ \frac{\partial F_1}{\partial A_n} & \frac{\partial F_1}{\partial B_m} \\ \frac{\partial F_1}{\partial A_n} & \frac{\partial F_1}{\partial B_m}\end{matrix}\right], \quad [\Delta X]=\left[\begin{matrix}\Delta A_n \\ \Delta B_m\end{matrix}\right],$$

$$[F]=\left[\begin{matrix}-F_1 \\ -F_2 \\ \vdots \\ -F_M\end{matrix}\right]$$

To get the solutions of Eq. (6) with the aid of ODLS method, we multiple the transposition of the matrix $[A]$ to get,

$$[A]^T[F]=[A]^T[A][\Delta X] \qquad (7)$$

where,

$$[A]^T[F]=[D]$$
$$[A]^T[A]=[C] \qquad (8)$$

Putting Eq. (6) into Eq. (7), we obtain the following.

$$[\Delta X]=[C]^{-1}[D] \qquad (9)$$

Summary of the process are shown in the below.

1. Gathering enough number of data from dynamic isochromatics.

2. Put arbitrary initial values of A_n, B_m into Eq. (4).

where, n=1~N and m=1~M, in this paper, N=M.

3. Calculate $[A]$, $[F]$

4. From Eq. (7), calculate ΔX.

5. Renew the values of A_n and B_m as the

following process.

$$[A_n]_{i+1}=[A_n]_i+\Delta A_n,$$
$$[B_m]_{i+1}=[B_m]_i+\Delta B_m$$

6. Reiterate the calculation until we get max $(\frac{\Delta X}{X}) \leq 0.00001$. If not, go back to step 3.

If the values of A_n and B_m are increasing in step 5, the calculation with the Newton-Raphson method is not converging but diverging. Preventing the calculation from resulting at wrong X values, we used $X_{i+1}=X_i+\delta\Delta X$. Where X_{i+1} is determined by minimum function, δ, when $[F_{i+1}]^T[F_{i+1}]$ is less than $[F_i]^T[F_i]$.

2.3 Regenerating dynamic isochromatic fringe-A hybrid experimental-theoretical procedure

Substituting the K_1 and K_2 extracted by the above procedure into Eqs. (1) and (2), we can regenerate dynamic isochromatic fringe patterns and compare the regenerated fringes with experimental results. By this final check process which we may call a hybrid experimental-theoretical procedure, we can confirm the right values of K_1 and K_2.

3. Experimental

3.1 Multi-spark camera system

The dynamic photoelasticity method consists of the Cranz-Shardin camera system with a multi-spark camera set, a dynamic photoelastic apparatus, a loading equipment, field lens and controllers as shown in Fig. 2. A general view of the experimental setup

The spark time delay can be controlled by using the start delay and horizontal·vertical delay in the range from 1μsec to 0.1sec for each frame. The pulse time to high speed camera frame is measured by using optical detecter to check the reliability of the framing rate. A time delay is setup to trigger the camera and oscilloscope signals at the moment when the aluminum tape attached behind the crack tip on the specimen is cut while the loading is increased by the manually operated oil jack.

3.2 Loading equipment

Figure 4 shows a mixed mode loading appara-
tus and it is possible to apply the mixed mode
load on DCB specimen by using two ton capacity
oil jack. The loading angle can be varied by
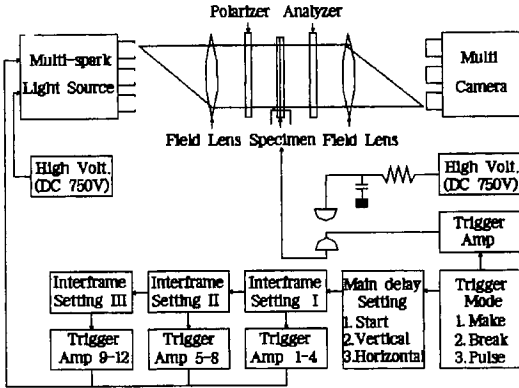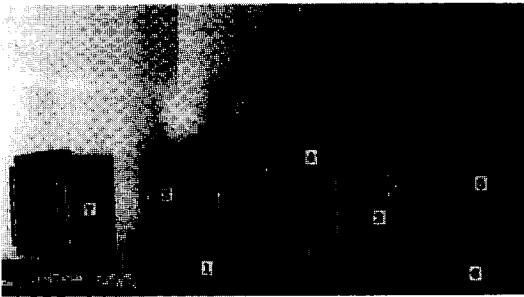changing the fixing holes in the angle changer.

Fig. 2 Block diagram of photoelasticity experimen-
tal setup

1. Polarizer 2. Analyser 3. Field lens 4. Loading apparatus
5. Multi-spark high speed light source 6. Trigger controller
7. Screem

Fig. 3 A general view of dynamic photoelasticity
experimental setup

When we manually operate the oil jack, the
connecting-rod is moving up to exert mixed mode
loading in the specimen.

3.3 Specimen and loading

Revealing the dynamic interface crack propaga-
tion phenomena and the dynamic stress field
surrounding the dynamically propagating inter-
facial crack tip, we manufacture specimens using
polycarbonate(PC) and aluminum(Al). After we
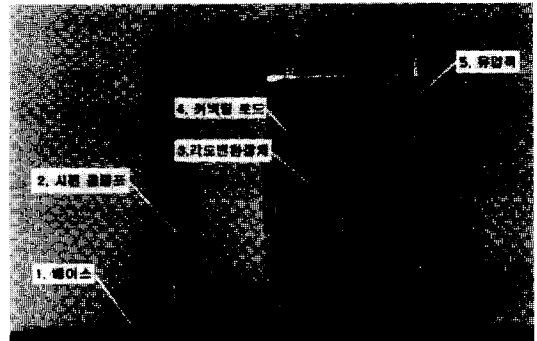clean up the interface of PC and Al, the halves are
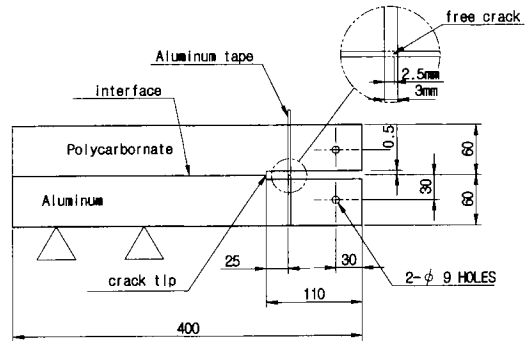

Fig. 4 Mixed mode loading apparatus

Fig. 5 Configuration of test specimen

Table 1 Material an physical properties of Polycarbonate and Aluminum

Property	Material	Polycarbonate	Aluminum
Poisson's ratio		0.38	0.33
Young's modulus, E(Gpa)		2.72	71.0
Material stress optics fringe value(MPa-mm/fr)		6.7	·
Shear modulus(Gpa)		0.98	·
Density (g/cm³)		1.196	2.80
Dilatational wave speed (m/s)		1960	6320
Distortional wave speed (m/s)		910	3100

bonded by epoxy and utilizer with the ratio of 1: 1. The interface thickness should be kept as 0.09 ~0.1mm. We use a comercial aluminum tape of width 3mm as a trigger band to initiate the camera. An 0.5mm single edge notch is introduced into the aluminum tape as shown in Fig. 5 to make it easy to be broken The residual stress along the interface is checked to be negligible by using a photoelasticity setup. The specimen thickness is 4.5mm.

The mechanical and physical properties of PC and Al-7075 are listed in Table 1.

4. Results and Consideration

Figure 6 shows the varying directions of mixed mode loadings which changes the load mixture ratio of y/x (vertical/horizontal) values. Three different y/x ratios such as 3.7(=F), 1.3(=F′) and 0.75 (=F″) are applied in the present study.

Figure 7 shows a typical full field dynamic isochromatics surrounding a dynamically propagating interface crack tip in the DCB specimen. Figures 8, 9 and 10. show the dynamic stress
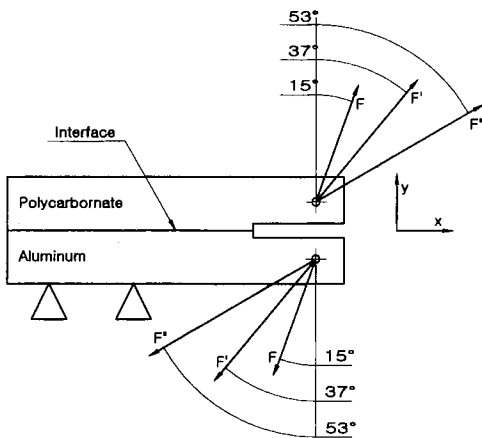
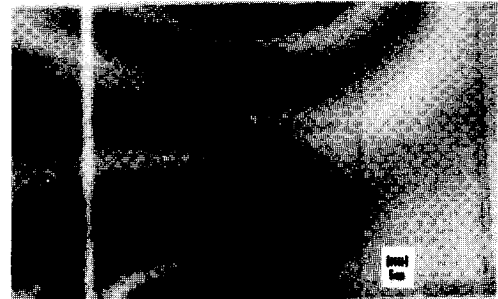**Fig. 6** Various mixtures of applied loads

Fig. 7 Typical dynamic isochromatic fringe patterns at a crack tip propagating along the interface in DCB specimen (crack runs left to right direction, scale: 1/0.7)
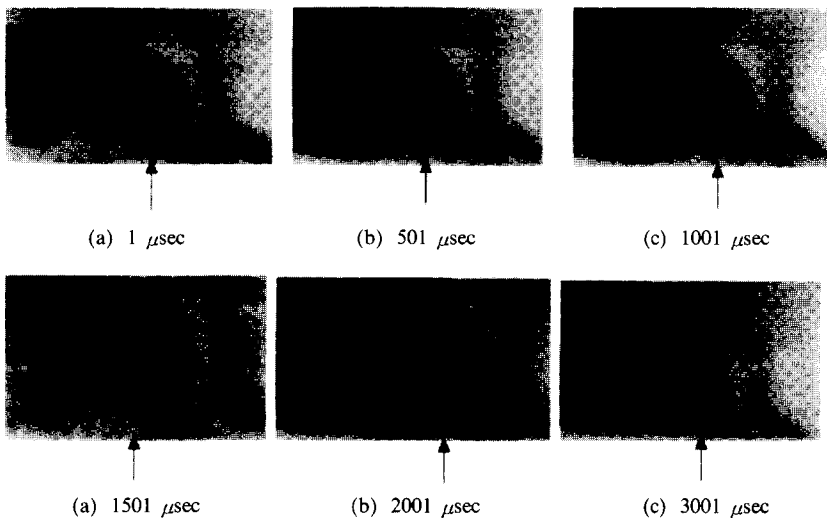

(a) 1 μsec   (b) 501 μsec   (c) 1001 μsec

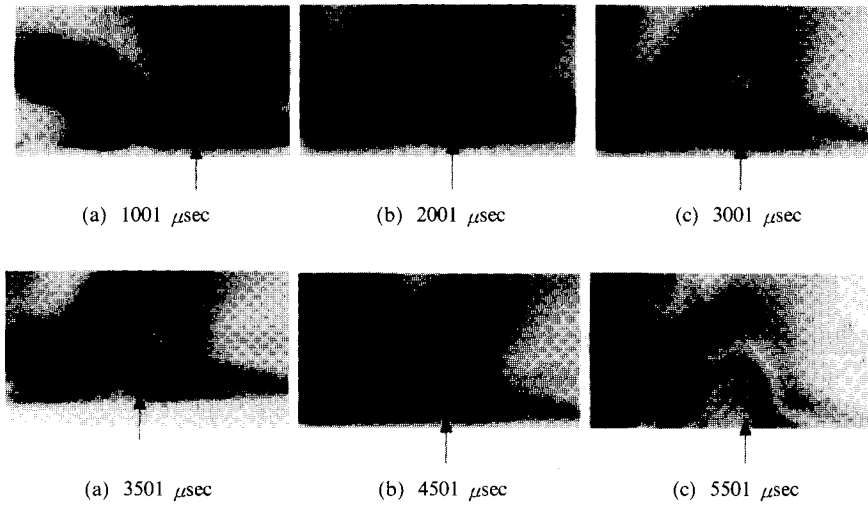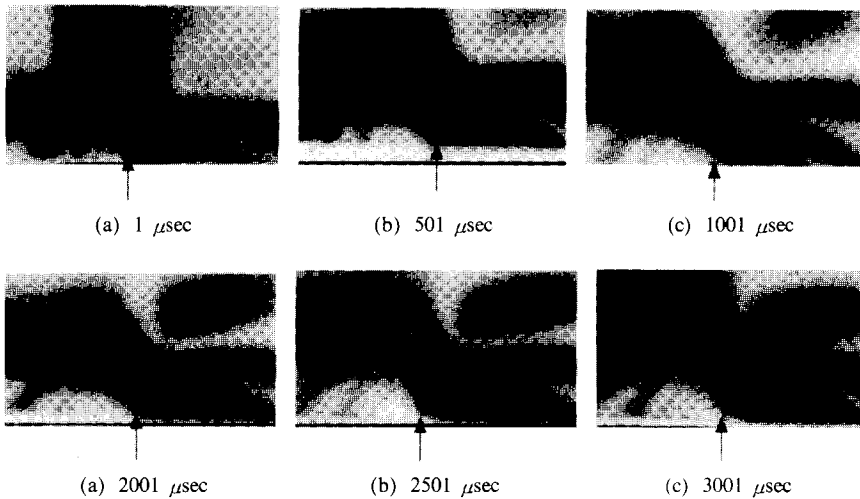(a) 1501 μsec   (b) 2001 μsec   (c) 3001 μsec

Fig. 8 Dynamic isochromatic fringe patterns in polycarbonate for a crack dynamically propagating along the interface by initial load F (crack runs left to right, scale: 4/1)
(μsec=time after break, ——→: propagating crack tip location)

(a) 1001 μsec   (b) 2001 μsec   (c) 3001 μsec

(a) 3501 μsec   (b) 4501 μsec   (c) 5501 μsec

Fig. 9 Dynamic isochromatic fringe patterns in polycarbonate for a crack dynamically propagating along the interface by initial load F′ (crack runs left to right, scale: 4/1)
(μsec=time after break, ⟶: propagating crack tip location)

(a) 1 μsec   (b) 501 μsec   (c) 1001 μsec

(a) 2001 μsec   (b) 2501 μsec   (c) 3001 μsec

Fig. 10 Dynamic isochromatic fringe patterns in polycarbonate for a crack dynamically propagating along the interface by initial load F″ (crack runs left to right, scale: 4/1)
(μsec=time after break, ⟶: propagating crack tip location)

field at the vicinity of the interface crack tip with varying loading condition such as F, F′ and F″, respectively. It is interesting to note that the initially mixed loading condition considerably affects the characteristics of isochromatic loop comparing to the results under the mode I loading condition obtained by Rosakis(Rosakis et al, 1998) and Shukla(Singh, 1996) groups in the USA.

Figure 11 summarizes the variation of crack velocities of dynamic interfacial cracks propagating under three different mixed loading conditions.

Comparing the crack propagating velocities for three different loads, we find that the crack propagating velocity decreases as y/x values (ranging from 3.7 to 0.75) becomes smaller. This implies that the crack propagating velocities get

faster when the part of mode I load increases as we may expect from the experimental results for the isotropic materials (Ramulu, 1982). However, the crack velocities for the dynamic interface

Fig. 11 Crack propagating velocites (C/C_R) vs. location of crack tip (C: crack propagating velocities C_R: Rayleigh wave velocity of polycarbonate)

fracture in the present study, which are about 7% of the Rayleigh wave speed of PC, are found to be very low comparing to other investigator's experimental results appeared in literatures (Singh & Shukla, 1996 ; Wang, Huang, Rosakis & Liu, 1998) which were measured mainly under mode I loading condition. More studies on the geometrical shape, thickness, the donding strength of the interface, the direction of mixed load and etc are, thus, needed to be done.

Figures 12, 13 and 14 show the comparison between the theoretical isochromatics and the experimental fringes on the quantitative aspect. The two isochromatic fringe loops agree well at the vicinity of the crack tips. Furthermore, it is found that K_1 and K_2 increase as y/x increases. The propagating crack velocities of about 7% of the Rayleigh wave speed of PC is found to be decreased. Therefore, more studies on the geomet-
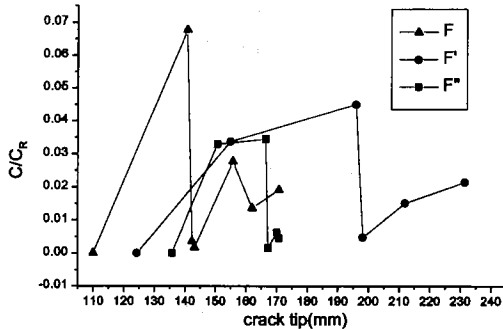
$K_1 : -1.608245, K_2 : 0.450180$

(a) 1 μsec

$K_1 : -1.607420, K_2 : 0.429493$

(b) 501 μsec

$K_1 : -1.608526, K_2 : 0.441253$

(c) 1001 μsec

$K_1 : -1.606250, K_2 : 0.424270$

(d) 1501 μsec

$K_1 : -1.610525, K_2 : 0.420244$

(e) 2001 μsec

$K_1 : -1.607559, K_2 : 0.425104$
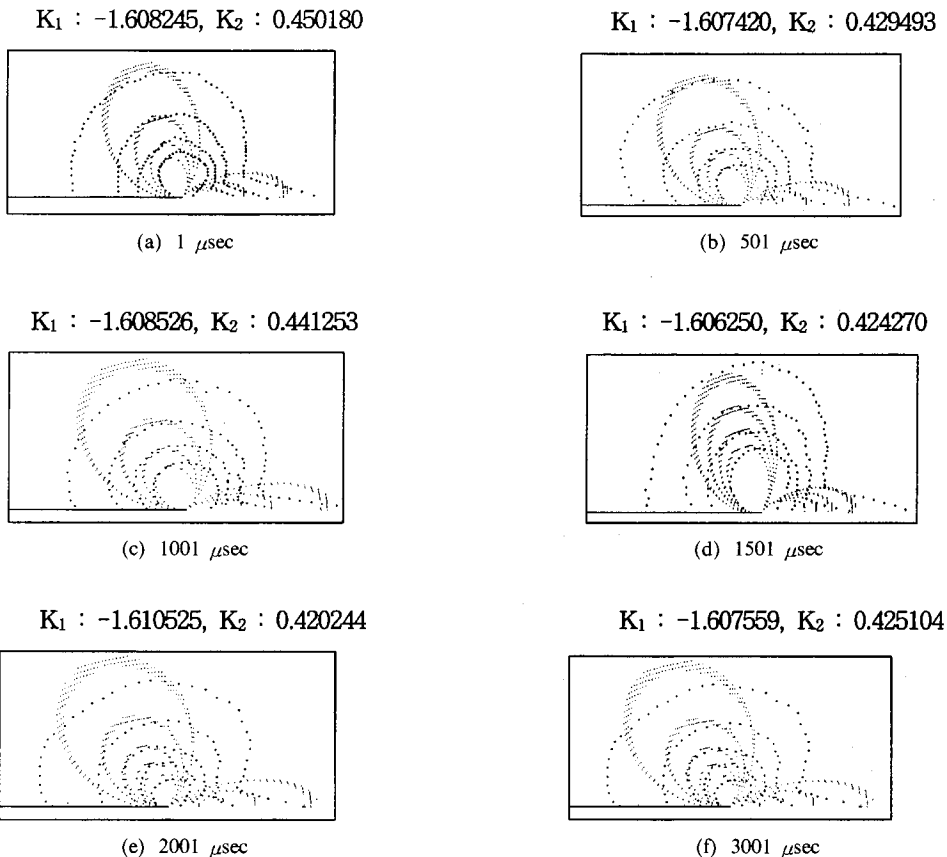

(f) 3001 μsec

Fig. 12 Theoretical and experimental isochromatic fringe patterns for a crack propagating along the interface by initial load F

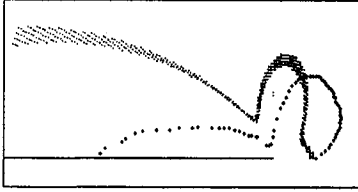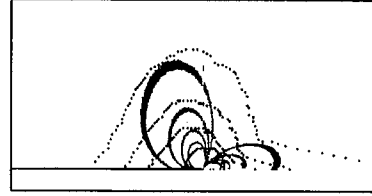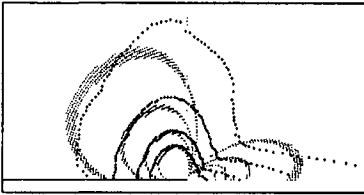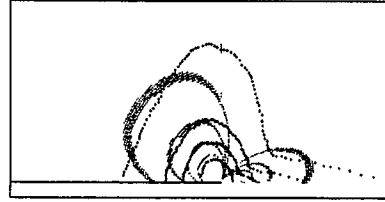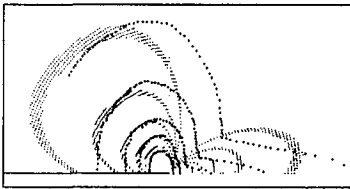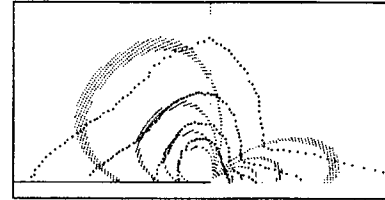$K_1 : -0.139491, K_2 : -1.963408$

(a) 1001 μsec

$K_1 : -1.801115, K_2 : 0.716241$

(b) 2001 μsec

$K_1 : -1.336133, K_2 : 0.757302$

(c) 3001 μsec

$K_1 : -1.352955, K_2 : 0.753905$

(d) 3501 μsec

$K_1 : -1.347988, K_2 : 0.753443$

(e) 4501 μsec

$K_1 : -1.358226, K_2 : 0.763198$

(f) 5501 μsec

Fig. 13 Theoretical and experimental isochromatic fringe patterns for a crack propagating along the interface by initial load F'

rical shape, thickness, the bonding strength of the interface, the direction of mixed load and etc are needed to be done.

The experimental and theoretical isochromatics agree well at the vicinity of the crack tips. However, it is noted that the errors are getting bigger as we compare the two at the location far from the crack tips where we need to incorporate the higher order effects.

The variation of K_1 and K_2 during dynamic interface crack propagating periods for DCB specimens under three different loading conditions are shown in Figs. 15, 16 and 17.

5. Conclusions

In this study, the dynamic mixed mode crack

propagation behavior for structural bonded interfaces are investigated by using a hybrid experimental-theoretical method with the aid of dynamic photoelasticity technique. The following results are obtained:

(1) The experimental and theoretical isochromatic fringe loops agree well at the vicinity of the dynamic interface crack tips. However, it is found that the errors are getting bigger as we collect the data at the locations far from the crack tips where the higher order coefficients are needed to incorporated.

(2) The dynamically propagating crack tip velocities of DCB specimen were of the order of about 7% of Rayleigh wave speed of PC. It is found that these are significantly small comparing to those obtained under the mode I impact load-
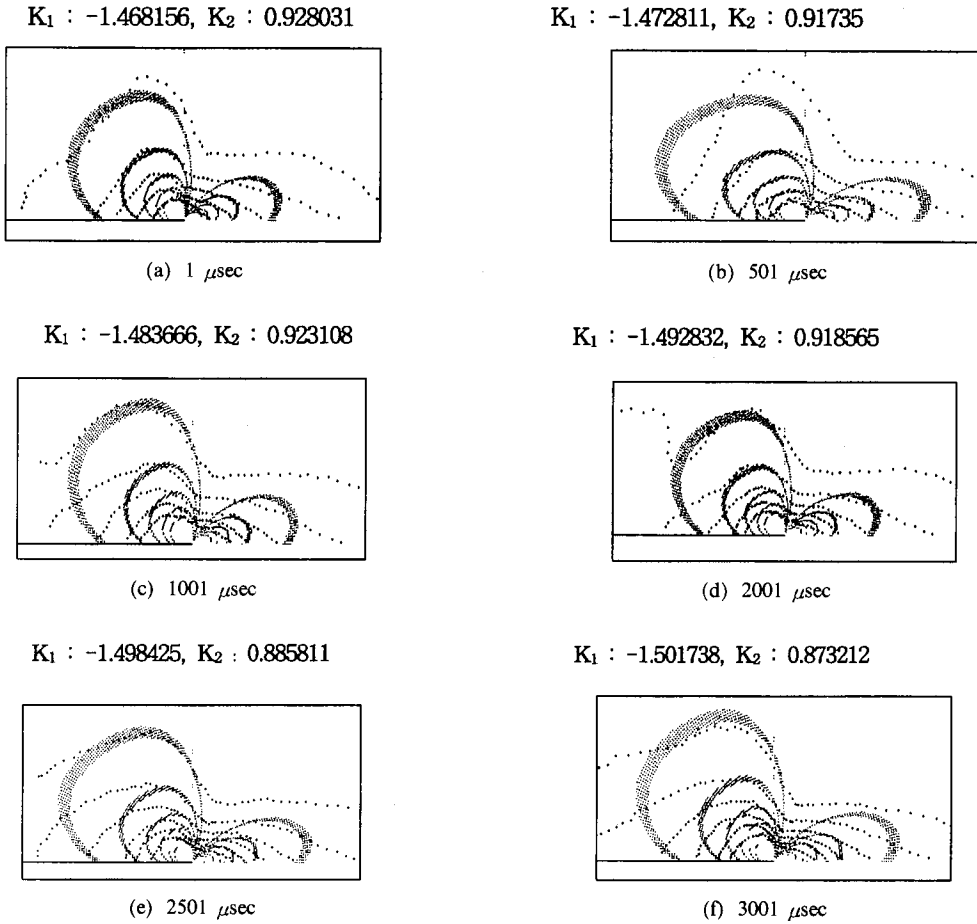
K_1 : -1.468156, K_2 : 0.928031

K_1 : -1.472811, K_2 : 0.91735

(a) 1 μsec

(b) 501 μsec

K_1 : -1.483666, K_2 : 0.923108

K_1 : -1.492832, K_2 : 0.918565

(c) 1001 μsec

(d) 2001 μsec

K_1 : -1.498425, K_2 : 0.885811

K_1 : -1.501738, K_2 : 0.873212

(e) 2501 μsec

(f) 3001 μsec

Fig. 14 Theoretical and experimental isochromatic fringe patterns for a crack propagating along the interface by initial load F''

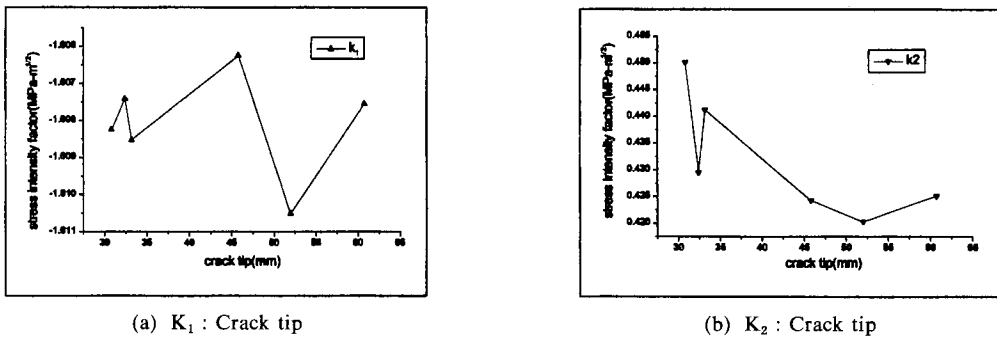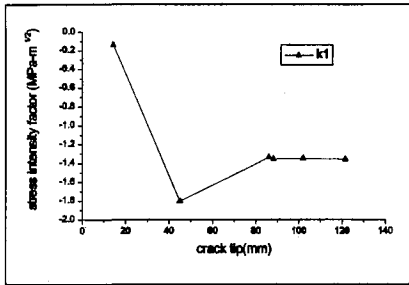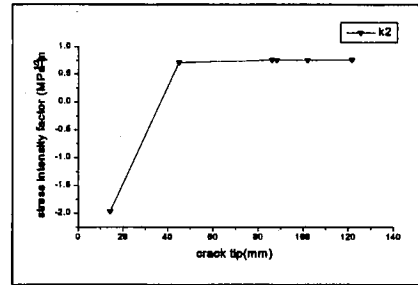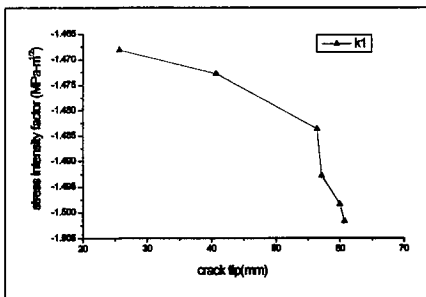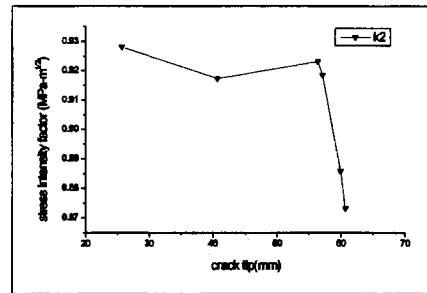(a) K_1 : Crack tip

(b) K_2 : Crack tip

Fig. 15 Stress intensity factor vs. Crack tip location by initial load F

ing condtions by Rosakis and Shukla in the USA. Therefore, it is suggested that more experimental studies pertaining the effects of geometrical shape, thickness, the bonding strength of the interface, the ratio of mixture of the load in structural joints

on dynamic interface crack propagation velocities should be carried out.

(3) The shapes of isochromatic fringes around the dynamically propagating interface crack tips under the mixed mode loading conditions are

(a) K_1 : Crack tip

(b) K_2 : Crack tip

Fig. 16 Stress intensity factor vs. Crack tip location by initial load F'

(a) K_1 : Crack tip

(b) K_2 : Crack tip

Fig. 17 Stress intensity factor vs. Crack tip location by initial load F''

very similar to ones obtained at the vicinity of the dynamic crack tip in the isotropic material under the mode II dominated loading condition.

Acknowledgment

References

Anderson, G. P., et al., 1977, *Analysis and Testing of Adhesive Bond*, Academic Press, New York.

Barber, J. R. and Comniou, M., 1983, *J. Appl. Mech.*, Vol. 50, pp. 770~776

Comninou, M., 1977, *J. Appl. Mech.*, E44, pp. 631~636.

Comninou, M., 1990, "An Overview of Interface Cracks," *Engineering Fracture Mechanics*, Vol. 37, pp. 197~208.

Dally, J. W. and Riley, W. F., 1991, *Experimental Stress Analysis*, McGraw Hill, pp. 424~506.

Deng, X., 1992, "Complete Complex Series Expansions of Near-Tip Fields for Steadily Growing Interface Cracks in Dissimilar Isotropic Materials," *Engineering Fracture Mechanics*, Vol. 42, No. 2, pp. 237~242.

Deng, X., 1993, "Genaral Crack-Tip Fields for Stationary and Steadily Growing Interface Cracks in Anisotropic Bimaterials," *Journal of Applied Mechanics*, Vol. 60, pp. 183~189.

Durelli, A. J. and Dally, j. W., 1975, "Stress concentration factors under dynamic loading conditions," *Jounal of Mechanical Engineering Science*, Vol. 16. No. 1, pp. 69~92.

Emery, A. F, et al., 1969, *Experimental Mechanics*, pp. 558~564

Gao, H., 1991, *J. Appl. Mech.*, vol. 58, pp. 931~168

Gdoutos, E. E., 1985, "Photoelasticity study of crack problems," *Photoelasticity in Engineering Practice*, Elseviser, London, pp. 181~204.

Gdoutos, E. E., et al, 1982, *Engineering Fracture Mechanics*, pp. 177~187

Gurtman, G. A. et al., 1965, *Experimental Mechanics*, Vol. 5, pp. 97~104

Kobayashi, A. S. and Mall, S., 1978, "Dynamic Fracture Toughness of Homalite-100," *Experimental Mechanics*, Vol. 18, No. 1, pp. 11~18.

Kokini, K., 1988, *ASME Trans., J. of Appl. Mech.*, Vol. 55, pp. 767~772

Kokini, K., et al., 1989, *Experimental Mechanics*, pp. 373~381

Lee, O. S. and Kim, D. Y., 1999, "Crack-Arrest Phenomenon of an Aluminum Alloy," *Mechanics Research Communications*, Vol. 26, No. 5, pp. 575~581.

Lu, H. and Chiang, F. P., 1993, *J. Appl. Mech.*, Vol. 60, pp. 93~100

Martin-Morgan et al., 1983, *J. Appl. Mech.*, Vol. 50, pp. 29~36

Mohammad, M. and Loren, Z., 1995, "Photoelastic Determination of Mixed Mode Stress Intensity Factors for Sharp Reentrant Corners," *Engineering Fracture Mechanics*, Vol. 52, No. 4, pp. 639~645.

Naik, R. A. et al., 1992, *NASA Report*.

Prendergast, P. J. 1996, *J. Bio. Engine*, Vol. 118, pp. 579~585

Ramulu, M, 1982, A Ph. D. Dissertation Submitted to the University of Washington, "Dynamic Crack Curving and Branching."

Rice., J. R. and Sih, G. C., 1965, "Plane Problems of Cracks in a Dissimilar Media," *ASME J. Appl. Mech.*, Vol. 32, pp. 418~423.

Rosakis, A. J., Samudrala, O., Singh, R. P. and Shukla, A., 1998, "Intersonic Crack Propagation in Bimaterial System," *Journal of Mechanics and Physics of Soilds*, Vol. 46, pp. 1789~1813.

Sanford, R. J., 1980, "Application of the Least Square Method to the Photoelastic Analysis," *Experimental Mechanics*, Vol. 20, pp. 192~197

Singh, R. P. and Shukla, A, 1996a, "Subsonic and Transonic Crack Growth along a Bimaterial Interface," *International Journal of Fracture*, Vol. 63, pp. 293~310.

Singh, R. P. and Shukla, A., 1996b, "Characterization of Isochromatics Fringe Patterns for a Dynamic Propagating Interface Crack," *International Journal Fracture*, Vol. 76, pp. 293~310.

Tsuji, M. et al., 1979, J., Therm. Str., 2, 215~232.

Wang, W. et al., 1998, "Effect of Elastic Mismatch in Intersonic Crack Propagation Along a Bimaterial Interface," *Engineering Fracture Mechanics*, Vol. 61, pp. 471~485.

Williams, M. L., 1959, "The Stresses around a Fault or Cracks in Dissimilar Media," *Bulletin of Seismological Society of America*, Vol. 49, No. 2, pp. 199~204

Xu, X. P. and Needleman, A., 1996, "Numerical Simulations of Dynamic Crack Growth along an Interface," *International Journal of Fracture*, Vol. 74, pp. 289~324.

Yang, W., Suo, Z and Shih, C. F., 1991, "Mechanics of Dynamic Debonding," *Proceedings of Royal Society of London, Series A*, Vol. 433, pp. 679~697.

Zhang, P. et al., 1989, Eng. Frac. Mech., Vol. 24, pp. 589~599